Réunion d'automne de la Société Suisse de Physique = Herbsttagung der Schweizerischen Physikalischen Gesellschaft = Autumn meeting of the Swiss Physical Society

Autor(en): **[s.n.]**

Objekttyp: **AssociationNews**

Zeitschrift: **Helvetica Physica Acta**

Band (Jahr): **70 (1997)**

Heft Sep. 2

PDF erstellt am: **27.09.2024**

Réunion d'Automne de la Sociéte Suisse de Physique

Herbsttagung der Schweizerischen Physikalischen Gesellschaft

Autumn Meeting of the Swiss Physical Society

October 10, 1997

La Chaux-de-Fonds, Switzerland

Helv. Phys. Acta 70, Separanda 2 (1997) S13 – S14
0018-0238/97/0200S13-02 $ 1.50+0.20/0

Helvetica Physica Acta

The Effect of Deliberately Induced Disorder on the Electronic Structure of the Bi-2212 High T_C Superconductor

I. Vobornik[+], C. Quitmann[§], M. Zacchigna[+], M. Grioni[+], R.J. Kelley[*], A. Karkin[&], M. Onellion[*], G. Margaritondo[+]

[+]*Institut de Physique Appliquée, EPFL, CH-1015 Lausanne,*

[§]*Experimentelle Physik 1A, Universitaet Dortmund, D-44221 Dortmund,*

[*]*Department of Physics, University of Wisconsin, Madison WI 53706, USA*

[&]*Institute for Metal Physics, Russian Academy of Sciences, 620219 Ekaterinburg GSP-170, Russia*

We have irradiated by thermal neutrons single crystals of the Bi-2212 high T_C superconductor. The irradiated samples are insulators, but they regain high T_C superconductivity after an annealing in He at 450-550°C. Depending on irradiation doses and annealing parameters, we obtained two insulators, with more or less disorder, and two superconductors with different values of T_C. We performed resistivity, a.c. susceptibility and angle resolved photoemission studies (ARPES). The coherent quasiparticle intensity in the vicinity of the chemical potential is considerably reduced in the insulating samples along both the Γ–M and Γ–Y high symmetry directions. It is recovered once the superconductivity is reestablished, and develops together with T_C along the Cu-O bond (Γ–M) direction.

The existence of the normal state gap - pseudogap was recently observed by angle resolved photoemission in underdoped high T_c cuprates [1]. However, it is important to distinguish between changes in spectral function related to the phenomenon of superconductivity from the changes related to the other properties of underdoped cuprates, namely to disorder [2]. Here, we report results obtained on thermal neutron irradiated single crystals of Bi-2212 high T_c superconductor. Original samples had T_c = 85 K. The irradiated samples were insulators. Superconductivity was recovered after a thermal annealing, as listed in Table 1). The motivation of our work was to investigate effects of disorder on spectral function, while keeping constant carrier concentration.

Irradiation [n/cm^2]	Annealing	Sample Type
$10 * 10^{18}$	/	Highly Disordered Insulator (HDI)
$5 * 10^{18}$	/	Less Disordered Insulator (LDI)
$10 * 10^{18}$	450°C for 45 min.	Lower T_C Superconductor (LTS) - T_C=40 K
$5 * 10^{18}$	550°C for 45 min.	Higher T_C Superconductor (HTS) - T_C=84 K

Table 1)

The angle resolved photoemission (ARPES) measurements were performed at the 4m - Normal Incidence Monochromator beamline of the Synchrotron Radiation Center at the University of Wisconsin. The spectra have been acquired along three high symmetry directions (Γ-X, Γ-Y, Γ-M) in the Brillouin zone, that were determined by Laue diffraction. At the photon energy of 21 eV, the uncertainty in k vector was ±0.037 A^{-1}. The total energy broadening (experimental and thermal) was 80 meV, as determined from an independently measured Fermi step of a metallic sample.

Fig. 1) illustrates angle resolved photoemission spectra taken at the same locations in the Brillouin zone for the four sample types along the Γ-M and Γ-X directions.

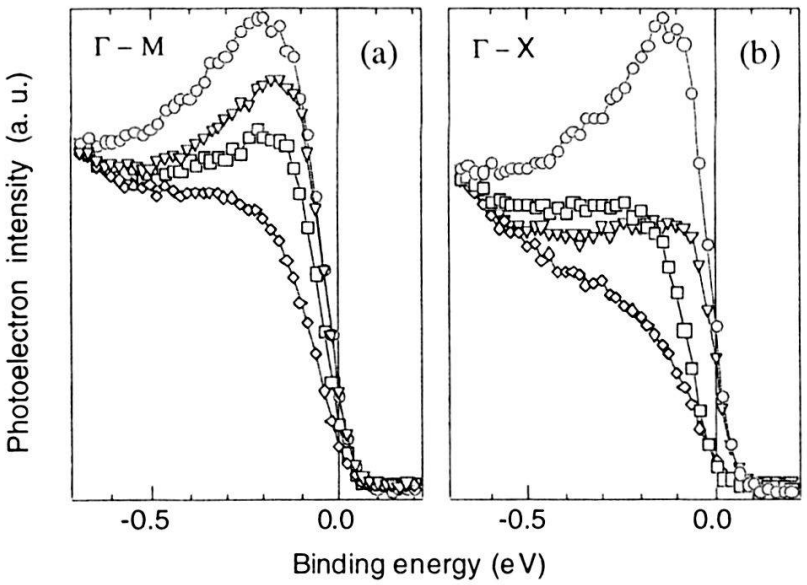

Fig. 1): Angle resolved photoemission spectra taken at the same locations in the Brillouin zone for the four sample types along the Γ-M (a) and Γ-X (b) directions.

—◇— HDI
—□— LDI
—▽— LTS
—○— HTS

The spectral intensity of the dispersing Bloch states is strongly suppressed in the case of the highly disordered insulator, and develops as the amount of disorder decreases. This development is uniform along the Γ-M direction, which corresponds to the Cu-O bonding direction in the real space, while along the Γ-X direction the lower T_c superconductor and the less disorder insulator exhibit almost the same spectral function. This indicates that T_c is especially sensitive to the behavior along the Γ-M direction in the Brillouin zone.

To summarize, one of the effects of irradiation-induced disorder in Bi-2212 is suppression of the spectral intensity of the dispersing Bloch states in the vicinity of the Fermi energy. Similar suppression of the spectral weight is observed in the underdoped cuprates when a pseudogap opens at $T>T_c$. These results are important for the interpretation of the ARPES data on underdoped Bi-2212, where doping achieved by chemical substitution unavoidably brings disorder into the system.

References:

[1] A. G. Loeser *et al.*, Science **273**, 325 (1996)

[2] C. Quitmann *et al.*, Phys. Rev. B **53**, 6819 (1996)

Helv. Phys. Acta 70, Separanda 2 (1997) S15- S16
018-0238/97/0200S15-02 $ 1.50+0.20/0

Helvetica Physica Acta

Positron polarimetry with $Nd_2Fe_{14}B$ magnets

C. Bee[a], J. Deutsch[b], J. Egger[c], W. Fetscher[a], J. Govaerts[b], M. Hadri[a], St. Kistryn[a], P. Knowles[b], J. Lang[a], O. Naviliat-Cuncic[a], R. Prieels[b], J. Sromicki[a], and P. van Hove[b]

[a] *Institut für Teilchenphysik, ETH-Zurich, CH-8093 Zurich*
[b] *Institut de Physique Nucléaire, UCL, B-1348 Louvain-la-Neuve*
[c] *Paul Scherrer Institut, CH-5232 Villigen*

The potential of using permanent $Nd_2Fe_{14}B$ magnets in a positron polarimeter has been explored with a beam of 50 MeV positrons. The asymmetries observed during a first test run provide encouraging results.

Several electron and positron polarimeters require a magnetized medium containing spin polarized electrons with appropriate orientation relative to the beam polarization component to be analyzed. Planar magnetized FeCoV (Vacoflux) foils have often been used in the past [1]. More recently, a substantial out-of-plane magnetization has been observed with Fe foils in a strong magnetic field [2]. Alternatively, an arrangement containing permanent magnets sandwiched between silicon strip detectors has been proposed as a compact and versatile polarimeter for electrons, positrons and photons but despite much effort, its sensitivity has not yet been established [3].

We present here the results of an exploratory experiment performed to assess the effectiveness of using out of plane magnetized $Nd_2Fe_{14}B$ magnets in a positron polarimeter employing both Bhabha scattering and annihilation in flight (AIF) reactions for the analysis of the longitudinal polarization of incident positrons [4]. The measurement was carried out in the πE3 beam channel at PSI. Positrons from μ-decay at rest in the production target were momentum selected at 50 MeV, with $\Delta p/p \approx 3\%$. The setup comprised four $36 \times 32 \times 1.8\ mm^3$ magnets mounted with adjacent pieces having opposite magnetization. Only plastic scintillators were used for the trigger in order to reduce scattering events originated from the surroundings of the magnets: four individual ($29 \times 29 \times 1.5\ mm^3$) and a common ($90 \times 90 \times 1.5\ mm^3$) detector were located upstream, in front of the magnets, to sign an incoming positron. A larger scintillator ($200 \times 200 \times 1.5\ mm^3$) was placed behind the magnets to identify the type of event. The polarimeter was completed by a BGO calorimeter constructed from 127 hexagonal modules to detect the scattering products (e^+e^- or $\gamma\gamma$). The front of the calorimeter was covered by two planes of 3 mm thick plastic hodoscopes used also in the trigger to sign the type of event. For comparison purposes, a magnetized iron foil tilted at 45° to the incident beam was used with a similar scintillators arrangement. From the time structure of the beam, measured at different momenta, the fraction of unpolarized positrons contributing to the trigger was estimated to be less than 10%.

In the off-line analysis, the gains of all detectors have been controlled and eventually adjusted. The presence of two well separated clusters on the calorimeter was required for Bhabha and AIF events, but just one for events corresponding to positrons not having interacted on the magnetized foil or permanent magnets, which were then used as normalization.

Normalizing the scattering events to the incoming positrons has been checked to give consistent results. Only events with a total energy equal to the initial incoming positron energy were further selected for the analysis. One of the permanent magnets broke during the run and its data has therefore been excluded.

The asymmetries under either field inversion or magnet rotation have been extracted. A common aspect of the results is the absence of an asymmetry signal for the events with the Bhabha trigger. This is suggestive of an insufficient selection of the true Bhabha events by the hardware and by the software cuts, and is under investigation with a Monte-Carlo calculation. However, a signal is apparent in the events with the AIF signature, with the expected inversion of sign for two adjacent magnets. More precisely, the two raw asymmetries measured for the AIF events were -0.026(7) and 0.015(6). For comparison, the asymmetry obtained with the tilted Fe foil was 0.020(4). Such low value is consistent with the incomplete saturation of the foils measured prior to the run. Unfortunately, no independent determination of the fraction of unpolarized background was made during the test in order to estimate the absolute analyzing power. In addition, one of the magnets does not present an asymmetry signal even for the AIF events. Nevertheless, as a first attempt the results are encouraging and indicate that permanent magnets merit further investigation.

References

[1] F. Corriveau *et al.*, Phys. Lett. **129B** (1983) 260; V.A. Wichers *et al.*, Phys. Rev. Lett. **58** (1987) 1821.

[2] L.J. de Bever, in Proc. 12th. Int. Symp. on High Energy Spin Physics, C.W. de Jager *et al.* eds., World Scientific, 1996, p.768.

[3] J.M. Hoogduin, PhD. thesis, Rijksuniversiteit Groningen, 1997 (unpublished).

[4] P. van Hove *et al.*, PSI proposal R-97-06.

Helv. Phys. Acta 70, Separanda 2 (1997) S17 – S18
0018-0238/97/0200S17-02 $ 1.50+0.20/0

Helvetica Physica Acta

Interface formation and chemical reactions on metal-GaTe(001) surfaces

J. Almeida, H. Berger and G. Margaritondo

Institut de Physique Appliquée, Ecole Polytechnique Fédérale, CH-1015 Lausanne, Switzerland

Abstract

We studied using x-ray photoelectron spectroscopy the deposition of Au, In, Ag and Al overlayers onto clean-cleaved GaTe(001) surfaces at room temperature. The first steps of the Schottky barrier formation on Au and In showed no interface reactions. Free Te release was observed after the deposition of 3.5 Å of silver. On the other hand, the deposition of Al leads to an exchange chemical reaction where clustering dominates at high metal coverage.

We present a x-ray photoemission spectroscopy study of metal on GaTe(001) surfaces. In contrast to others anisotropic semiconductors, there are reported only a few photoelectron spectroscopy investigations on GaTe surfaces. Gallium telluride crystallizes in a monoclinic structure formed by layers bound between themselves by weak van der Waals bonds. Each layer consists of four atomic planes, Two anions planes in the outside and two cations plane in the middle. The elementary unit cell of GaTe contains six formula units with 12 atoms, in difference with hexagonal III-VI layer compounds as GaSe and GaS.[1]

The samples were cleaved in-situ at a base pressure better than 5×10^{-10} mbar, and gold, indium, silver or aluminum was evaporated on samples at room temperature. Photoemission spectroscopy studies were performed using a Scienta ESCA-300 system at the EPFL Centre de Spectromicroscopie. This system is equipped with an Al Kα radiation source at 1486.6 eV, a x-ray monochromator and a concentric hemispherical analyzer. The intensity of the photon source is estimated to be 20 W sr/mm^2 and the energy resolution was better than 0.3 eV, as derived from the Fermi edge of a clean Ag surface.

We calculated the Schottky barrier height ϕ_{B_p} from the position of the Ga3d doublet relative to E_F using the relation

$$\phi_{B_p} = (\mathrm{Ga}_{3d-VBM}) - \mathrm{Ga}_{3d}$$

The term (Ga_{3d-VBM}) is the position of the Ga3d core level relative to the gallium telluride valence band maximum edge, which was derived from a linear fit of the edge data on fresh cleaved samples. The zero of the binding energy scale is referred to the Fermi level position E_F of the spectrometer.

We characterized the clean-cleaved GaTe(001) surfaces by measuring the Ga3d and Te4d peaks, and the valence band. The Ga3d core level was deconvolved in a huge bulk peak at a binding energy of 18.9 eV and a surface component at +0.36 eV. The full width at half maximum (FWHM) value of these peaks was 0.56 eV. The values of the branching ratio B and spin-orbit splitting Δ_{SO} were 0.67 and 0.45 eV and were kept constant for all the Ga3d spectra measured. On the other hand, the Te4d core level was deconvolved with only one doublet having fitting parameters of 0.73 eV FWHM, B= 0.69 and Δ_{SO}= 1.44 eV. The valence band maximum (VBM) edge position was derived from a linear fit of the edge data, giving a cut off position at 0.35 eV. After these values, the distance between the Ga3d and the VBM is 18.55 eV, and at the samples' surface the Fermi level is located 0.33 eV above the VBM.

The deposition of Au lead to a shift of the Ga and Te core levels by 0.11 eV to higher binding energies. A similar behavior was observed after the deposition of In, leading to a band bending change of 0.25 eV in the same direction. In these two cases, no significant lineshape change occurs after metal deposition indicating the absence of interfacial reactions. The extra doublet at -0.8 eV from the Ga3d peak has the same parameters than the Ga level. This component is not related to substrate-overlayer exchange reactions, but it has been previously correlated with surface Ga atoms which are in contact with the deposited In atoms.[2] The shift of this component with respect to the bulk level is associated to a final state effect due to screening of the hole in the surface Ga atom by the neighboring In atoms. For In coverage $\Theta<6$ Å, the valence band spectrum was unchanged throughout this region. For higher Θ values, the valence band spectra show emission near the Fermi level indicating the presence of metallic clusters.

The aluminum deposition on the clean-cleaved p-type GaTe(001) surface produced a rigid shift (band bending) of about 0.43 eV to higher binding energies which stabilizes for a ≈4 Å thick overlayer. The formation of the Al-GaTe interface includes a cation exchange reaction. In this case, a peak of the cation (Ga) gave evidence of a metallic phase.[3] A new feature identified as metallic Ga, is located at ≈ -0.88 eV respect to the bulk peak and shows a marked asymmetry, characteristic of the Doniach-Sunjic line shape for metallic species. Its intensity grows up to reach 25% of the bulk Ga3d peak at ≈35 Å Al deposition.

Silver deposition on the cleaved GaTe surface produced a band bending shift of 0.24 eV to higher binding energies. During the formation of the Ag-GaTe interface, the presence of no significant lineshape change after metal deposition suggests the absence of interfacial reactions. On the contrary, some evidence for the presence of a overlayer-substrate interaction was given from inferences about the interface morphology by examining the dependence of the peak intensities on overlayer coverage thickness. When Ag is deposited on GaTe, we observe that in the Te4d/Ga3d intensity ratio remains constant with the same exponential attenuation, and the Ag3d intensity increases rapidly. These facts suggest an initial 2D growth up to 1.8 Å. From this thickness value, the Ag3d peak intensity continues increasing and starts to saturate at about 3.5-4 Å indicating that the Ag clustering is the dominating mechanism. From this last thickness value, we observe also that the Te4d intensity increases much faster than the Ga3d. This fact indicates tellurium outdifussion, some kind of reaction involving Te and Ag is forming at the interface.

The Schottky barrier height values, as determined by XPS in function of metal coverage are presented in figure 1. The weak dependence of barrier height on metal work function suggests that a high density of interface states are responsible of the Fermi-level pinning.[4]

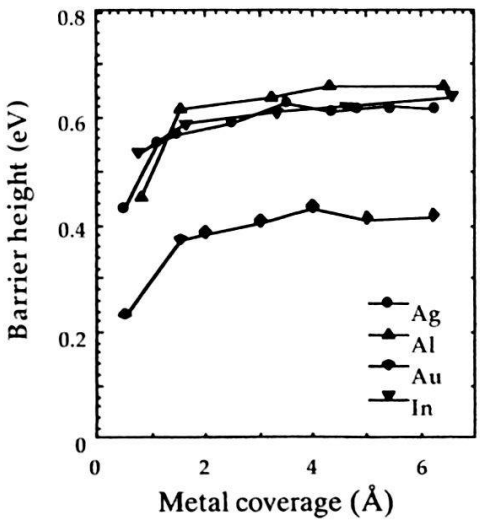

FIG. 1

References

[1] F. Hulliger, *Structural Chemistry of Layer-type Phases*, F. Levy ed. (D. Riedel, Boston, 1976).

[2] M. Alonso, R. Cimino, Ch. Maierhofer, Th. Chassé, W. Braun and K. Horn, J. Vac. Sci.Tecnol. **B8** (4), 955 (1990).

[3] D. Mao, A. Kahn, G. LeLay, M. Marsi, Y. Hwu, G. Margaritondo, M. Santos, M. Shayegan, L. T. Florez and J. P. Harbison, J. Vac. Sci. Technol. **B9** (4), 2083 (1991).

[4] D. Pal, S. Pal and D. Bose, Solid St. Commun. **97**, 725 (1996).

Helv. Phys. Acta 70, Separanda 2 (1997) S19 – S20
0018-0238/97/0200S19-02 $ 1.50+0.20/0

Helvetica Physica Acta

Unusual spectral signatures of organic 1D metals

F. Zwick[1], M. Grioni[1], M. Onellion[2], G. Margaritondo[1]
[1]*Institut de Physique Appliquée, EPFL, CH-1015 Lausanne*
[2]*Department of Physics, University of Wisconsin, Madison WI 53706, USA*

We have studied by high resolution angle resolved photoelectron spectroscopy the spectral properties of two metallic and one insulating Bechgaard salts, quasi-1D organic materials. The spectra of the metals show no dispersing quasiparticle peak crossing the Fermi level. Instead a deep pseudogap is observed. The spectral lineshape is incompatible with that of "normal" metals. The spectrum of the insulator exhibits a real energy gap.

We investigated the electronic structure of the quasi one-dimensional (1D) organic compounds $(TMTSF)_2X$ ($X=PF_6$, ClO_4) and $(TMTTF)PF_6$ by angle resolved photoelectron spectroscopy (ARPES). These materials are characterized by linear chains formed by the stacking of planar molecules, and their physical properties are strongly anisotropic. The overlap of the molecular orbitals leads to a development of coherent states along the chains, with strong electronic correlations [1]. All three materials are 1D metals at RT, but their ground states are different. $(TMTSF)PF_6$ develops a spin density wave (SDW) below 12K. $(TMTSF)_2ClO_4$ is a superconductor at ~1 K. Electronic correlations in $(TMTTF)PF_6$ leads to charge localization and a metal-insulator transition at ~200 K.

At the Wisconsin Synchrotron Radiation Center we measured high quality single crystals mounted on a cold stage and cleaved in UHV to expose a clean (001) surface. The temperature was 150 K. We used linearly polarized synchrotron radiation ($h\nu$=20 eV) and a 50 mm hemispherical analyzer. The angular resolution was <1° and the energy resolution 70 meV (including thermal broadening).

Fig. 1 shows the ARPES data for $(TMTSF)_2ClO_4$, along the chain direction. Analogous results are obtained for $(TMTSF)_2PF_6$. We observe three non dispersive peaks at 4, 2.5 and 1 eV, and additional intensity linearly decreasing towards the Fermi level. The intensities of the three features strongly depend on the polarization of the photon beam, as expected for 1D states [2]. The spectral weight at the Fermi level is weak throughout the Brillouin zone, and

indicates a deep pseudogap, already suggested by angle-integrated spectra [2]. Fig. 2 compares high resolution spectra of metallic $(TMTSF)_2ClO_4$ and insulating $(TMTTF)PF_6$. The leading edge of the insulating compound is shifted by 100±20 meV towards higher binding energy, indicating a real charge gap. The observed value is in good agreement with optical measurement of the gap [3].

The suppression of spectral weight at E_F, and the lineshape of the ARPES spectra are clearly incompatible with a Fermi liquid picture. They may be consistent with a Luttinger liquid scenario, which should be relevant for these materials, with a large characteristic exponent. None of the present theoretical models, however, can naturally explain the absence of dispersion.

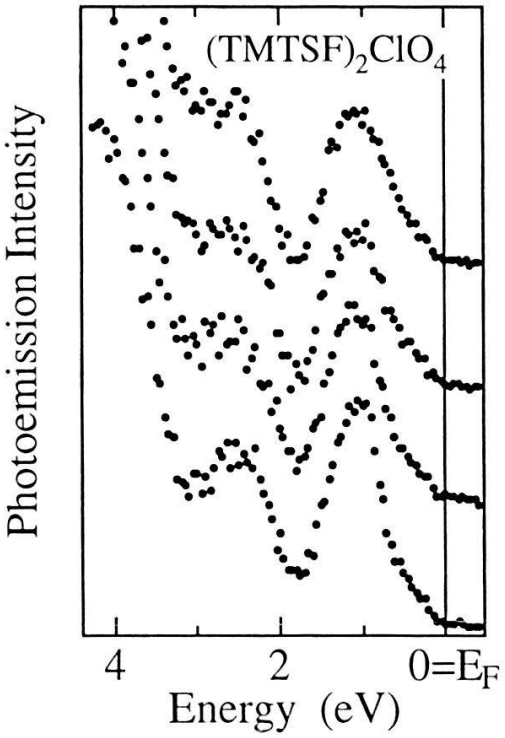

Fig. 1. ARPES spectra of $(TMTSF)_2ClO_4$, along the 1D chain direction. The bottom spectrum was measured at Γ, and the top at the zone boundary.

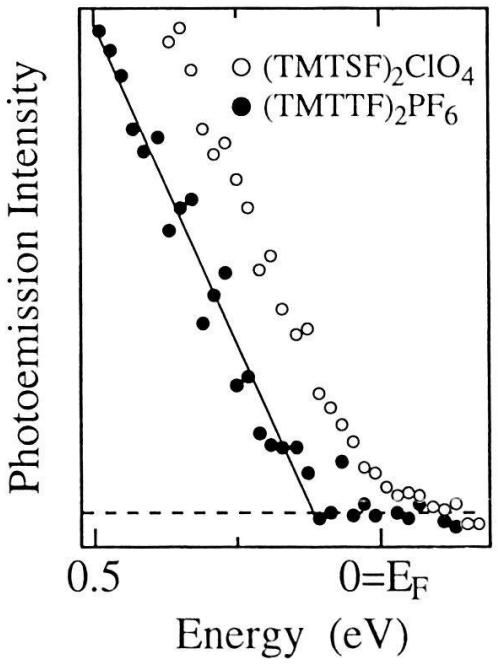

Fig. 2. High resolution ARPES spectra of $(TMTSF)_2ClO_4$ and $(TMTTF)_2PF_6$. The energy shift reveals a real gap of ~100 meV in the latter.

References:

[1] D. Jérome, Science **252**, 1059 (1991).
[2] B. Dardel et al., Europhys. Lett. **24**, 687 (1993).
[3] M. Dressel et al., Phys. Rev. Lett. **77**, 398 (1996).

Helv. Phys. Acta 70, Separanda 2 (1997) S21 – S22
0018-0238/97/0200S21-02 $ 1.50+0.20/0

Helvetica Physica Acta

Upper Hubbard Band of the 2-D Hubbard Model

Walter Zimmermann[1], Raymond Frésard[2], and Peter Wölfle[1]

[1]Institut für TKM, Postfach 6980, Universität Karlsruhe, D-76128 Karlsruhe
[2] Institut de Physique, A-L Breguet 1, CH-2000 Neuchâtel

We calculate the one-electron Green's function of the Hubbard model on the square lattice using a spin-rotation invariant six-slave boson representation. In the strong coupling regime its spectrum splits off into a quasi-particle peak, and a lower and an upper incoherent branch, which we focus on, using a functional integral formulation. By including Gaussian fluctuations around a paramagnetic saddle-point, we obtain the main contributions to G as the graphs which are of lowest order in the fluctuations, in the strong coupling regime. The k-dependence of the weight of the upper band shows the physically expected behavior. We also find that its total weight quickly decreases away from half-filling under an increase of the hole doping.

The calculation of the spectral function of the 2-d Hubbard Model remains a serious challenge despite of decades of work. Its relevance to the understanding of the High T_c-superconductors has been repeatedly emphasized in the literature. The strong correlation effects have so far been elucidated in various limits, such as the large space dimensionality limit [1], or in one dimension, but the 2-d and 3-d systems keep on escaping our understanding. In these systems even highly sophisticated self-consistent schemes, such as FLEX fail to even qualitatively reproduce the splitting of the non-interacting band into lower and upper bands [2]. In this work we resort to the Spin-Rotation-Invariant slave-boson approach [3], which naturally splits off the low energy and high energy incoherent excitations, on top of the quasi-particle peak.

In this approach the creation operator of a physical electron $c^+_{i,\sigma}$ is written in terms of auxiliary bosons e, p_μ, d and fermions $f^+_{i,\sigma}$ as: $c^+_{i,\sigma} = \frac{1}{2}\sum_{\mu,\sigma'}\left(e_i p^+_{i,\mu}\tau^\mu_{\sigma,\sigma'} + d^+_i \sigma\sigma' p_{i,\mu}\tau^\mu_{-\sigma',-\sigma}\right) f^+_{i,\sigma}$. In order to evaluate the Green's function $G_{i,j,\sigma}(\tau) = -T < c_{i,\sigma}(\tau)c^+_{j,\sigma}(0) >$ we expand the slave-bosons around their mean-field amplitudes. Doing that to quadratic order in the action yields the propagators of the slave-bosons and constraints fields, which can be gathered from [4]. We now concentrate on the high energy excitations. In the strong coupling regime they are described by the d-boson. The lowest order contributions to the Green's function are given by:

$$G(\vec{k},\omega)_{High} = \frac{\Pi(\vec{k},\omega) + \Pi_{p_z}(\vec{k},\omega) + \Pi_{p_0}(\vec{k},\omega)}{1 - t_{\vec{k}}(\Pi(\vec{k},\omega) + \Pi_{p_z}(\vec{k},\omega) + \Pi_{p_0}(\vec{k},\omega))} \tag{1}$$

where $t_{\vec{k}}$ is the dispersion of the non-interaction band and the various $\Pi's$ are defined in Fig. 1. Please note that they also contain the appropriate vertices.

We now discuss the numerical results. The calculations have been performed for $U = 25t$ and $\beta t = 2.5$, where the paramagnetic phase does not show any kind of instability. We postpone the detailed discussion of the spectral function and density of states to a separate publication. In short the spectral function exhibits a strong $\vec{k}$-dependence. It is typically

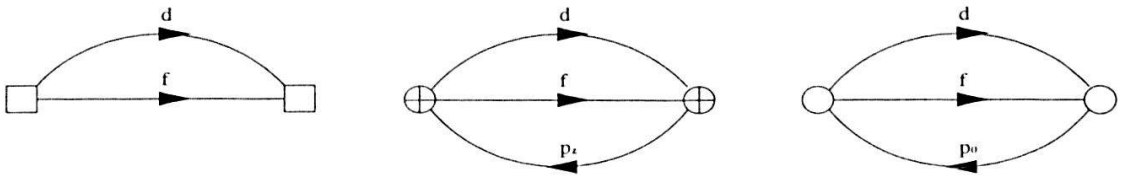

Figure 1: From left to right: $\Pi(\vec{k},\omega)$, $\Pi_{p_z}(\vec{k},\omega)$ and $\Pi_{p_0}(\vec{k},\omega)$

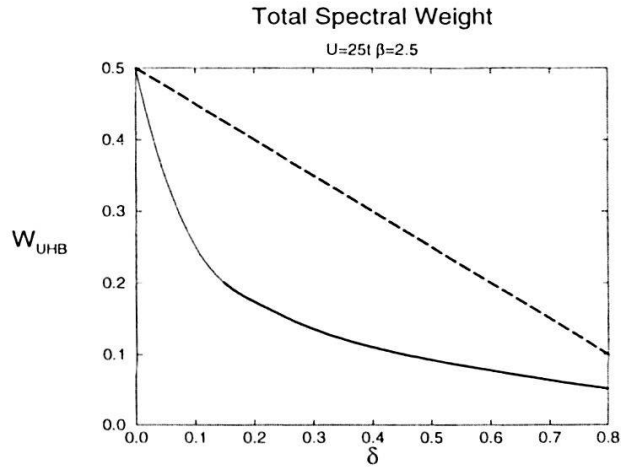

Figure 2: Total weight, SB calculation(full line) and $t-J$ model sum rule(dashed line).

large for wave-vectors in the vicinity of the Fermi surface, and small otherwise. It is smallest at the band center. This is expected since the states are occupied. Its width in frequency is mostly k-independent, and close to the bare band-width. All the main features of the exact diagonalization results are reproduced by our approximation [5]. The doping dependence of the total weight of the upper Hubbard band W_{UHB} is shown on Fig. 2. It is seen to fall off quickly under a decrease of the density. The decay is substantially larger than what one may expect from the sum-rule of the $t-J$ model. This is in agreement with the numerical data of Eskes and Olès [6]. In summary we applied for the first time the SRI slave-boson formulation of the Hubbard model to the calculation of the Green's function away from half-filling. Our results are in good agreement with known numerical data. This work has been supported by the Deutsche Forschungsgemeinschaft through Sonderforschungsbereich 195. One of us (RF) is grateful to the Fonds National Suisse de la Recherche Scientifique for financial support under Grant 8220-0284525.

References

[1] A. Georges *et. al.*, Rev. Mod. Phys. **68**, 13 (1996).
[2] Y.M. Vilk and A.-M.S. Tremblay, cond-mat/9702188
[3] R. Frésard and P. Wölfle, Int. J. Mod. Phys. B **6**, 685 (1992).
[4] W. Zimmermann, R. Frésard and P. Wölfle, Phys. Rev. B **56**, (1997) (at press).
[5] E. Dagotto and A. Moreo, Phys. Rev. Lett. **67**, 14 (1991).
[6] H. Eskes and A.M. Olès, Phys. Rev. Lett. **73**, 9 (1994).

Helv. Phys. Acta 70, Separanda 2 (1997) S23 – S24
0018-0238/97/0200S23-02 $ 1.50+0.20/0

Helvetica Physica Acta

ANISOTROPIC OPTICAL MATRIX ELEMENT OF QUANTUM WIRES OBTAINED WITH ANALYTICAL EIGENSTATES

F. Filipowitz, F.-K. Reinhart

Institute of Micro- and Optoelectronics, Federal Institute of Technology, CH-1015 Lausanne, Switzerland

Abstract : Analytical valence band eigenstates, including valence band mixing, are obtained for rectangular quantum wires with infinite barriers, in the spherical approximation. The optical matrix element of quantum wire interband transitions are evaluated with this new approach.

Theoretical predictions[1] showed that quantum wires (QWR) should have better optical properties (higher gain or absorption due to the discontinuity in the joint density of states) then quantum well or bulk materials. Usual numerical evaluation of the absorption of QWR structures is complicated due to the non negligible valence band mixing. In this article we propose a novel approach, valid in the spherical approximation, to evaluate valence band states. Analytical valence band eigenstates for rectangular quantum wires with infinite barriers, including band mixing, can be found with this method.

Valence band eigenstates, usual approach:
In the spherical approximation, the Luttinger parameters obey $\gamma_2 = \gamma_3 = \bar{\gamma} \neq \gamma_1$. The valence band hamiltonian[2] of electrons close to the Γ_8 symmetry point is then given by $\mathbf{H_v} = \frac{1}{m_0} \cdot \left\{ \frac{1}{2} \cdot \left[\gamma_1 + \frac{5}{2} \bar{\gamma} \right] \mathbf{p}^2 - \bar{\gamma} \frac{1}{\hbar^2} \cdot (\mathbf{p} \cdot \mathbf{J})^2 \right\} + U(\mathbf{r})$ [Eq.(1)], where $\mathbf{p}$ is the momentum operator, $\mathbf{J}$ the angular momentum operator ($J = 3/2$), $U(\mathbf{r})$ the heterostructure valence band potential, and m_0 the free electron mass. The usual approach to solve the Schrödinger equation, $\mathbf{H_v}[\Psi] = \varepsilon \cdot \Psi$ [Eq.(2)], is to project this equation on the basis $\left\{ e^{i\mathbf{k}\cdot\mathbf{r}} \bullet \left| J_z^\sigma \right\rangle \right\}$, where $\left| J_z^\sigma \right\rangle$ is a state representing the periodic part of the Bloch function. Its angular momentum along the z direction, has the value of $\sigma = \pm 3/2, \pm 1/2$. There is valence band mixing, if the wave vector is not aligned along the z-direction, even in the case of non confined structures. Due to this mixing, valence band eigenstates must be evaluated numerically for quantum confined structures.

Valence band eigenstates, alternative approach:
We propose a novel approach to evaluate valence band eigenstates, including the band mixing effects by projecting Eq.(2) onto the basis $\left\{ e^{i\mathbf{k}\cdot\mathbf{r}} \bullet \left| J_\mathbf{k}^\sigma \right\rangle \right\}$. The state $\left| J_\mathbf{k}^\sigma \right\rangle$ represents the periodic part of the Bloch function whose angular momentum along the $\mathbf{k}$ direction has the value of $\sigma = \pm 3/2, \pm 1/2$. It is obtained by a rotation of $\left| J_z^\sigma \right\rangle$, explicitely given in Ref.3[3]. The envelope function for heavy hole (HH) and light hole (LH) are solution of the envelope Schrödinger equation $\left[\frac{\hbar^2}{2 \cdot m_{eff}} \cdot \nabla^2 + U(\mathbf{r}) \right] F^H(\mathbf{r}) = E \cdot F^H(\mathbf{r})$, (H= HH or LH), [Eq.(3)], where

$m_{eff} = \frac{m_0}{\gamma_1 - 2\bar{\gamma}}$ [Eq.(4)] is the HH effective mass. The sign inside [Eq.(4)] is changed for the LH effective mass. It can be shown that the projection of Eq.(3) onto the basis $\left\{e^{i\mathbf{k}\cdot\mathbf{r}}\right\}$ gives the same elements as the projection of Eq.(2) onto the basis $\left\{e^{i\mathbf{k}\cdot\mathbf{r}} \bullet \left|J_{\mathbf{k}}^{\sigma}\right\rangle\right\}$, if $\sigma = \pm 3/2$ ($\sigma = \pm 1/2$) correspond to the heavy (light) hole envelope function. The Fourier transform of the envelope function, $\tilde{F}^H(\mathbf{k})$, gives these elements. Therefore $F^H(\mathbf{r}) = \int \tilde{F}^H(\mathbf{k}) \cdot e^{i\mathbf{k}\cdot\mathbf{r}} d^3\mathbf{k}$ and $\Psi^{\sigma}(\mathbf{r}) = \int \tilde{F}^H(\mathbf{k}) \cdot e^{i\mathbf{k}\cdot\mathbf{r}} \cdot \left|J_{\mathbf{k}}^{\sigma}\right\rangle d^3\mathbf{k}$ are solutions of Eq.(3) and Eq.(2), respectively.

Application to a rectangular quantum wire:
The valence and conduction fondamental states of a rectangular QWR with cross-section L_x x L_y and infinite barriers have been evaluated with the novel approach. Eq.(5) gives the analytical expression of its fundamental valence band state, including the so called band mixing effects.

$$\Psi_{k_z}^{\sigma}(x,y,z) = \frac{e^{ik_z \cdot z}}{\sqrt{L_z}} \left[\int G_{L_x}(k_x) \cdot G_{L_y}(k_y) \cdot \left| J_{(k_x,k_y,k_z)}^{\sigma} \right\rangle \cdot e^{i(k_x \cdot x + k_y \cdot y + k_z \cdot z)} \, dk_x dk_y \right] \quad \text{[Eq.(5)]}$$

where for $L=L_x$ or L_y $G_L(k) = \frac{\sqrt{2L}}{\pi^2 - k^2 \cdot L^2} \cdot \cos\left(\frac{L}{2} \cdot k\right)$ and $\sigma = \pm 3/2, \pm 1/2$. The electron wave vector and the wire length are $\mathbf{k}=(k_x,k_y,k_z)$ and L_z, respectively.
The Fig.1 and Fig.2 show the optical matrix element of the lowest energy electron to heavy hole (E1-HH1) and the corresponding E1-LH1 transition of a 200 x 50 Å QWR as a function of k_z. The three cases of light polarization parallel to x, y or z are given.

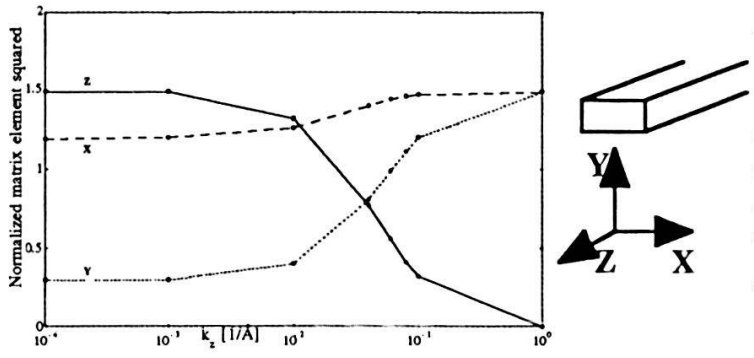

Fig.1: Normalized absolute square of the optical matrix element for the E1-HH1 transition of a 200 x 50 Å quantum wire. X, Y and Z indicates the polarization of the light vector.

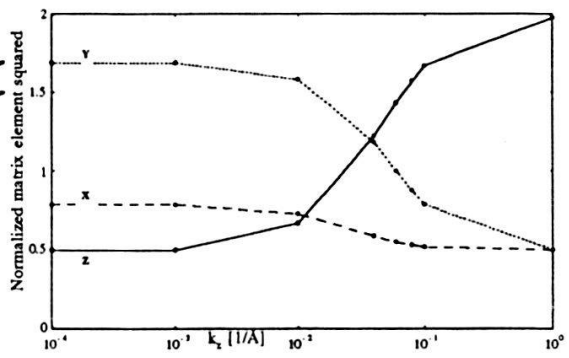

Fig.2: Normalized absolute square of the optical matrix element for the E1-LH1 transition of a 200 x 50 Å quantum wire. X, Y and Z indicates the polarization of the light vector.

References:
[1]D.A.B. Miller, D.S. Chemla and S. Schmitt-Rink, Appl. Phys. Lett., **52**, 2154-2156 (1988)
[2]J.M. Luttinger, Phys. Rev., **102**, 1030-1041 (1956)
[3]E.O. Kane, J. Phys. Chem. Solids, **1**, 249-261 (1957)

Helv. Phys. Acta 70, Separanda 2 (1997) S25 – S26
0018-0238/97/0200S25-02 $ 1.50+0.20/0

Helvetica Physica Acta

First-Principles Calculation of Electric-Field Gradients at the Cu Sites in $YBa_2Cu_3O_7$

P. Hüsser, S. Schafroth, E. Stoll, H.U. Suter, and P.F. Meier

Physik-Institut, Universität Zürich-Irchel, 8057 Zürich

The electric-field gradients at the Cu sites in $YBa_2Cu_3O_7$ have been investigated using first-principles cluster procedures. For the planar Cu, a large cluster comprising 74 atoms was studied with both Hartree-Fock and density functional methods. The latter calculations provide field gradients and asymmetry parameters in good agreement with the experimental values for hydrostatic pressures up to 0.6 GPa.

Nuclear magnetic and quadrupole spectroscopy has provided a considerable amount of data on both static and dynamic properties of high-temperature superconductors. In particular, the electric-field gradient (EFG) has been determined for a variety of nuclei (e.g. Cu(1) and Cu(2) in $YBa_2Cu_3O_7$) with high accuracy [1]. Theoretical approaches to calculate the EFG at the Cu(2) site on the ab initio level[2, 3] failed to predict the experimental value[4].

Therefore we calculated the EFGs by using appropriate large clusters and more suitable basis sets. The density functional (DF) method was applied using both the local density approximation (LDA)[5] and the generalized gradient approximation (GGA)[6]. These results are compared with Hartree-Fock (HF) calculations.

To determine the electric field gradients at a specific lattice site it is necessary to choose a cluster that is centered appropriately. For the Cu(1) site in $YBa_2Cu_3O_7$, calculations with a rather small cluster (Cu_3O_{12}) yield EFGs in good agreement with the experiments. For Cu(2), however, a considerably larger cluster ($Cu_{12}O_{42}Y_{12}Ba_8$) is needed. It contains 74 atoms and is centered around the midpoint between two adjacent Cu(2) sites along the c direction. This cluster has zero charge and is, in addition, embedded in 2448 point charges.

method	Cu(1) V_{bb}	η	Cu(2) V_{cc}	η
UHF[a]	11.2	0.3	-22.2	0.04
LAPW[b]	7.4	0.8	-5.6	0.07
HF	28.53	0.04	-20.73	0.09
DF/LDA	7.49	1.00	-15.76	0.00
DF/GGA	7.12	0.94	-16.17	0.01
experiment[c]	7.51±0.03	0.99	-12.35±0.02	0.01

Table 1: Theoretical and experimental EFGs (in 10^{21} Vm^{-2}) and asymmetry parameters at Cu(1) and Cu(2) in $YBa_2Cu_3O_7$. a) Ref. [2], b) Ref. [3] and c) Ref. [4]

The calculated EFGs at the Cu sites obtained with HF and the DF methods are given in Table 1, together with previous theoretical values and experimental data [4].

For Cu(1), our calculated EFG values are in agreement with previous theoretical studies. For Cu(2) [7], the EFGs are closer to the experimental value than those obtained with earlier theoretical approaches [2, 3].

Furthermore, the pressure dependence of the EFG at the Cu(2) site was determined varying the lattice parameters [8]. This simulation of the influence of hydrostatic pressure is in good agreement with NQR experiments [9] (Fig. 1).

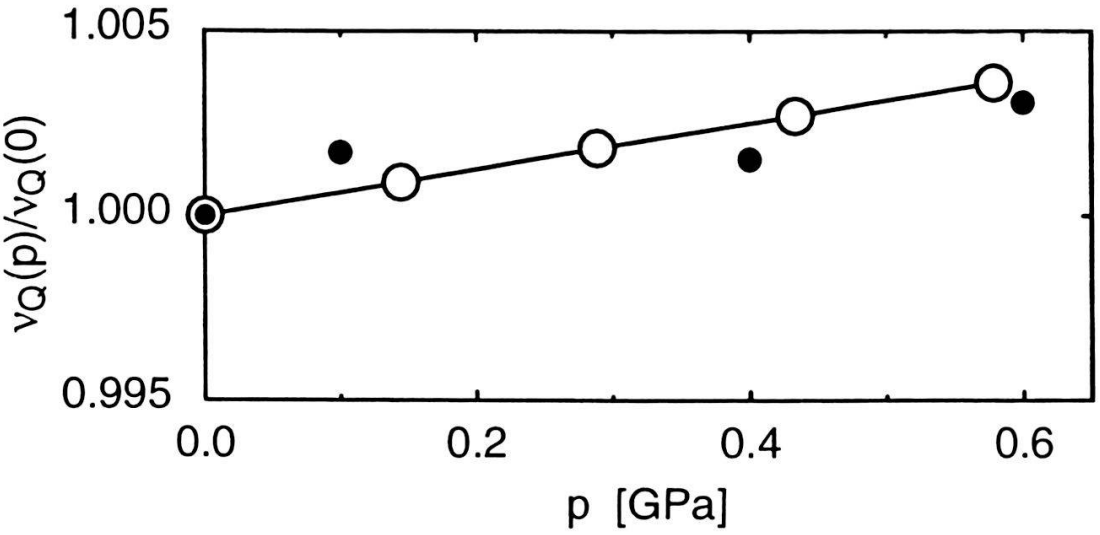

Figure 1: Normalized pressure dependent NQR frequencies $\nu_Q(p)/\nu_Q(0)$. • experiments of Ref. 9. ○ our DF/GGA calculations.

We like to thank D. Brinkman, M. Mali, and J. Roos for valuable discussions. This work is partially supported by the Swiss National Science Foundation. One of us (P.H.) thanks the Centro Svizzero di Calcolo Scientifico in Manno for hospitality during the Project Related Student Stages in Summer 1995.

References

[1] For a review, see D. Brinkmann and M. Mali, NMR Basic Principles and Progress, (Springer, Heidelberg, 1994), Vol 31, p 171.

[2] N. Sahoo, S. Markert, T. P. Das, and K. Nagamine, Phys. Rev. B**41**, 220 (1990).

[3] K. Schwarz, C. Ambrosch-Draxl, and P. Blaha, Phys. Rev. B**42**, 2051 (1990).

[4] C. H. Pennington, D. J. Durand, C. P. Slichter, J. P. Rice, E. D. Bukowski, and D. M. Ginsberg, Phys. Rev. B**39**, 2902 (1989).

[5] S. H. Vosko, L. Wilk and M. Nussair, Can. J. Phys., **58**, 1200 (1980).

[6] A. D. Becke, Phys. Rev. A**38**, 3098 (1988).

[7] P. Hüsser, E. Stoll, H.U. Suter, P.F. Meier, Physica C (1997) (in press).

[8] J.D. Jorgensen, S. Pei, P. Lightfoot, D.G. Hinks, B.W. Veal, B. Dabrowski, A.P. Paulikas, and R. Kleb, Physica C, **171**, 93 (1990).

[9] K. Müller, M. Mali, J. Roos, and D. Brinkmann, Physica C, **162-164**, 173 (1989).

Helv. Phys. Acta 70, Separanda 2 (1997) S27 - S28
0018-0238/97/0200S27-02 $ 1.50+0.20/0

Helvetica Physica Acta

Test of QED and the Size of Fundamental Particles

A. Hasan, J. Ulbricht and J. Wu

Eidgenössische Technische Hochschule, ETH Zürich, CH-8093 Zürich, Switzerland

Total and differential cross sections for the process $e^+e^- \to \gamma\gamma(\gamma)$, and the total cross section for the process $e^+e^- \to \gamma\gamma\gamma$, are measured at energies around $\sqrt{s}$= 91 GeV and 130-140 GeV using the data collected with the L3 detector from 1991 to 1996. We set lower limits, at 95% CL, on a contact interaction energy scale $\Lambda > 695$ GeV on the mass of an excited electron $m_{e^*} > 174$ GeV and on the QED cut-off parameters $\Lambda_+ > 177$ GeV and $\Lambda_- > 170$ GeV. An empirical model about the the size of fundamental particles is also discussed.

Total and differential cross sections for the process $e^+e^- \to \gamma\gamma(\gamma)$, and the total cross section for the process $e^+e^- \to \gamma\gamma\gamma$, are measured at energies around $\sqrt{s}$= 91 GeV and 130-140 GeV using the data collected with the L3 detector from 1991 to 1996. Fig.1 shows the measured differential cross section and the QED calculations normalized to the Born level and to radiative effects up to $O(\alpha^3)$.

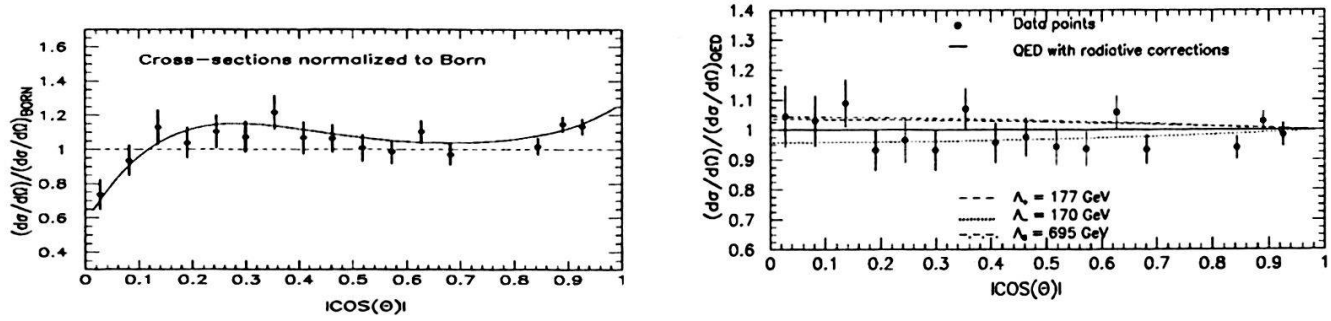

Figure 1: Differential cross section normalized to Born level and QED $O(\alpha^3)$ level.

The agreement between the data and the QED predictions (fig.1) is used to constrain the existence of an excited electron of mass m_{e^*} which replaces the virtual electron in the QED process [1] or a model with deviation from QED arising from an effective interaction with non-standard $e^+e^-\gamma$ couplings and $e^+e^-\gamma\gamma$ contact terms [1] . The analysis delivers in the first case $m_{e^*} > 174$ GeV with the QED cut-off parameters $\Lambda_+ > 177$ GeV and $\Lambda_- > 170$ GeV [1] and in the second case a cut-off parameter limiting the geometrical diameter of the interaction area to $\Lambda > 695$ GeV (2.8×10^{-17} cm).
This analysis and the CDF [2] data exclude excited electrons below 170 GeV and excited quarks from 80 GeV to 760 GeV. The limits for the direct contact term measurements of this analysis, ref. [3] and the g-2 experiments [4] are in the range 10^{-17}cm - 10^{-24} cm. As in the QED it seems that the fundamental particles (FP) have no internal substructure and their size is down to zero. With some uncertainties for the neutrino masses this would mean that the density of the FP in a classical framework would be infinite at diameter zero. Before this limit is reached, the radius of FP must cross a Schwarzschild black hole radius (SBHR), e.g the electron has the SBHR at 1.4×10^{-57} m. A black hole has mass, spin and electric charge like FP but its stability is questionable if the diameter is below 10^{-13} cm.

For the following discussion we consider a scenario where a quantized object exists which is stable down to the rest masses of the FP. We further assume that the four interactions between these quantized black holes (QBH) are linked to the four orthogonal coordinates in space and time. Strong, electromagnetic and weak interaction are space-like and gravity is time-like.

Such a QBH would be defined by the four interactions and limited in size by a boundary. This allows to separate every coordinate in three areas to place charges around the QBH. For example left side, center and right side of the QBH; or outside, on the boundary and inside the QBH; or left side, on the boundary and right side of the QBH. We used the first case to assume: the charges of the strong interaction are the three colors (C), for the electromagnetic interaction $Q = \pm 1/3$, for the weak interaction $T_3 = \pm 1/2$ and for the gravity $+m$ for matter and $-m$ for antimatter. These two assumptions allow us to write down a scheme of representation for all the fermions and bosons. Fig.2 shows an example for the electron. The left side of fig.2 connects the space coordinates to the charges T_3, Q ,C and the right side connects the time to the mass. The integrated charge for a worm-hole-like geometrical object is also shown. Such an object would have the degree of freedom to develop a discrete mass spectrum via oscillation or rotation. As all fermions have the same spin, in a pure empirical attempt a highly degenerated and elliptically deformed oscillator potential is used to describe the mass spectra of the fermions.

$E(n_x, n_y, n_z; Q) = (A + BQ + CQ^2 + DQ^3)(n_x + n_y + n_z)^{R+S(Q+1)Q(Q-1)+T((Q+1)Q(Q-1))^2}$

A comparison of masses between experiment and this empirical model is shown in fig.2.

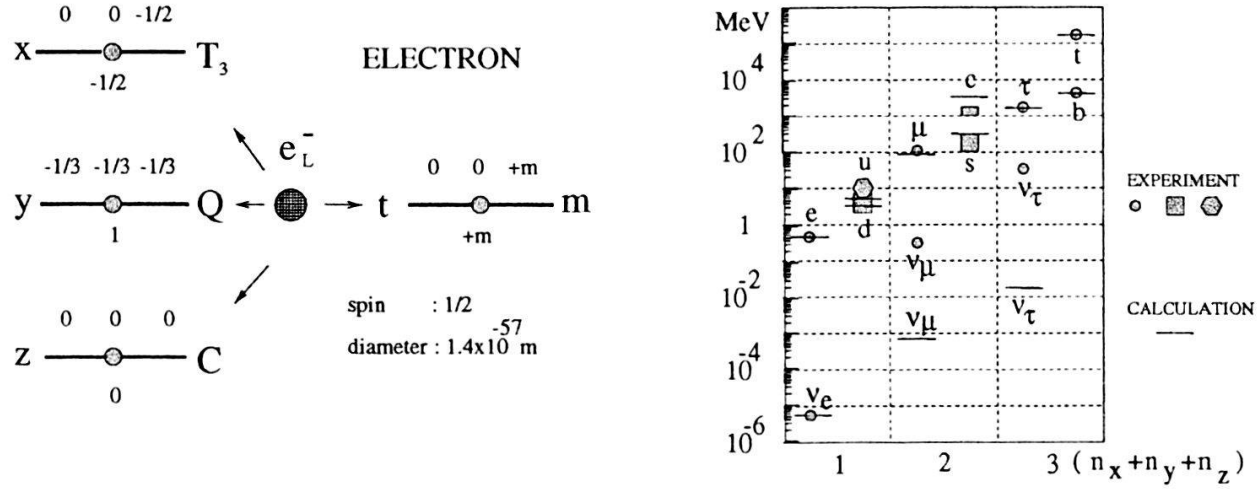

Figure 2 : A scheme for the electron charges (left) and mass spectra of the fermions (right).

Three free parameters, $n_{x,y,z} = 0, 1, 2, 3..$, and the fermion charges $Q = 0, -1/3, 2/3, -1$ have been used in the calculation. The constant factors $A = 5.1 \cdot 10^{-6}$ MeV, $B = -8.5$ MeV, $C = 10.8$ MeV, $D = 18.7$ MeV, $R = 7.42, S = -4.34$ and $T = 4.15$ are obtained by fitting to the data.

References

[1] L3 Collab.,M.Acciarri et.al.,Phys.Lett.B**384** (1996)323,
J.Wu, USTC-Hefei, Ph.D Thesis (1997) unpublished.
[2] F.Abe et.al.Phys.Rev.D **55** R5263 (1997)
[3] OPAL Collab.,G.Alexander et.al.Phys.Lett.B **387** (1996)432
[4] P. Mery et.al.Z.Phys.C **46** (1990)229